ROYAL SOCIETY
OF CHEMISTRY

COMMUNICATION

Check for updates

From nanofibers to ordered ZnO/NiO heterojunction arrays for self-powered and transparent UV photodetectors†

Zhiming Zhang, Yi Ning and Xiaosheng Fang ⓘD *

Uniformly aligned electrospun nanofiber arrays are important building blocks for high-performance functional devices and device arrays. However, it remains a challenge to prepare perfectly aligned and large area nanofiber arrays using common electrospinning. In this work, a modified electrospinning method utilizing three assisted electrodes for nanofiber collection was proposed to achieve uniformly aligned and millimeter-long ZnO and NiO nanofiber arrays (more than 90% of nanofibers aligned to within $\pm 4°$ of the desired direction), which were further fabricated into ZnO/NiO heterojunction arrays with a density of 10^6 cm^{-2}. Photodetectors (PDs) based on the as-prepared ZnO/NiO heterojunction arrays exhibited excellent ultraviolet (UV) selective and self-powered detection properties because of the properly matched energy bands of ZnO and NiO. A maximum responsivity of 0.415 mA W^{-1} and a short rise/decay time of 7.5 s/ 4.8 s at 0 V bias of the device markedly outstripped the reference ZnO nanofiber array device. The three-assisted-electrode electrospinning method of this work offers new chances in novel nanostructure design and high-performance device fabrication.

Introduction

The controlled assembly of nanomaterials has proved to be a powerful way of fabricating high-performance functional devices.[1–5] Electrospinning, as a convenient and low-cost nanomaterial fabrication method, has been widely applied in preparing aligned nanofiber arrays.[6–8] Recently, electrospun nanofiber arrays prepared using assisted electrodes as collectors have found application in PDs,[9,10] supercapacitors,[11,12] strain sensors[13] and so on.[14] Nevertheless, the imperfect alignment of electrospun nanofibers in these works creates a large number of crossing defects which restricts the improvement of device performance as well as the realization of device arrays;[15] meanwhile, these reports usually focus on only one kind of nanofiber, which limits

further construction of complex nanostructures and functional devices. Thus, a universal electrospinning method that can prepare uniformly aligned nanofiber arrays of different materials is urgently needed.

ZnO is one of the most widely studied nanomaterials for UV PDs because of its proper bandgap of 3.37 eV and easy fabrication.[16,17] However, pure ZnO nanomaterial based PDs often suffer from slow response speed which is determined by oxygen adsorption and desorption on the surface of ZnO.[18,19] To solve this problem, combining ZnO with other materials to form heterojunctions is one of the most promising avenues to achieve high-speed UV PDs.[20–22] On the one hand, there are a wide range of candidates having properly matched energy bands with ZnO which can speed up the charge separation process of photo-generated carriers. On the other hand, hetero-junctions with a built-in electric field also have the potential to realize self-powered PDs.[23,24] When the self-powered PDs work without external bias, the input light also serves as their power supply, and thus change of input light will lead to a fast change of device current.

Herein, we proposed a modified electrospinning method using three assisted electrodes to regulate the orientation of nanofibers. With this method, nanofibers of several millimeters long with more than 90% aligned to within $\pm 4°$ of the desired direction were prepared. To demonstrate the application of this method, we prepared uniformly aligned ZnO and NiO nanofiber arrays. Next, highly ordered ZnO/NiO heterojunction arrays with a density of 10^6 cm^{-2} were successfully fabricated and constructed into highly-selective UV PDs. Benefiting from its built-in electric field, the ZnO/NiO heterojunction array PD showed greatly improved self-powered characteristics (a maximum respon-sivity of 0.415 mA W^{-1} and a short rise/decay time of 7.5 s/4.8 s at 0 V bias) compared with a reference ZnO nanofiber array device. Meanwhile, an average transmittance of 90% in the visible light region was also achieved for the ZnO/NiO heterojunction array PD. Our demonstration of this high-performance ZnO/NiO PD proved the ability of three-assisted-electrode electrospinning in preparing ordered nanostructures for high-performance electronic devices.

Department of Materials Science, Fudan University, Shanghai 200433, P. R. China.
E-mail: xshfang@fudan.edu.cn

This journal is © The Royal Society of Chemistry 2019

J. Mater. Chem. C, 2019, 7, 223–229 | 223

Experimental

Preparation of ZnO and NiO nanofibers

For the preparation of ZnO nanofibers, 0.45 g polyvinylpyrrolidone (PVP, M_n of 1.3×10^6) was dissolved in 3 g ethanol and 0.4 g zinc nitrate hexahydrate was dissolved in 1 g deionized water. The two kinds of solution were then mixed by magnetic stirring for several hours to obtain a viscous sol, and then transferred into a 5 mL syringe with a steel needle tip of 0.41 mm inner diameter. The positive bias connected to the needle tip and the negative bias connected to the substrate were 10 kV and -2 kV, respectively. The distance between the needle tip and the substrate was 15 cm, and the feeding speed of the precursor was 0.02 mm min^{-1}. The relative humidity of the surroundings was kept below 35%. After electrospinning, the as-prepared nanofibers were calcined in air for 1 h at 520 °C at a heating rate of 1 °C min^{-1} to finally achieve ZnO nanofibers. For the preparation of NiO nanofibers, nickel nitrate hexahydrate was used instead of zinc nitrate hexahydrate while other operations were kept the same.

Preparation of ZnO/NiO heterojunction arrays

Square glass slides of 0.8 cm × 0.8 cm were used as substrates. For the preparation of roughly aligned nanofibers, two parallel aluminum foils with a 0.9 cm gap were used as assistant electrodes and the substrate was placed between them. A negative voltage of -2 kV was connected to the two aluminum foils. For the preparation of ZnO/NiO heterojunction arrays, a third aluminum foil electrode of 0.5 cm width was inserted in the middle of the former two electrodes with the substrate placed on it. The third electrode was grounded while the two outside electrodes were still connected to a negative voltage of -2 kV. The substrate was covered in advance using a handmade paper shadow mask with a 0.8 cm × 0.4 cm rectangular window in the middle. Uniformly aligned ZnO nanofiber arrays were first electrospun on the substrate for 30 s (before calcination, the composition of nanofibers was actually PVP containing $Zn(NO_3)_2$). After this, the paper shadow mask was removed along with the nanofibers present on it, and ZnO nanofiber arrays deposited through the window were left on the substrate. NiO nanofiber arrays were then prepared using the same method but in the perpendicular direction to the ZnO nanofibers. After calcination, the cross points of ZnO and NiO nanofibers formed ZnO/NiO heterojunction arrays in the middle of the substrate. The surrounding ZnO and NiO nanofibers were also kept so that the Cr/Au electrodes for the electronic and optoelectronic property study could be deposited on them.

Fabrication of devices

Cr/Au (30/70 nm) electrodes were deposited on the as-prepared nanofibers *via* electron beam evaporation using a handmade paper shadow mask. For the ZnO/NiO heterojunction arrays, the paper shadow mask had two separated rectangular window of 0.4 cm × 0.1 cm and the position of the corresponding electrodes is illustrated in the inset of Fig. 3a. For both ZnO and NiO nanofiber arrays, Cr/Au electrodes of the same size with ZnO/NiO heterojunction arrays were utilized. The configuration of the electrodes is illustrated in the inset of Fig. 3b, and the distance between the electrodes was 0.6 cm.

Characterization and measurements

Optical images were taken using a metallographic microscope equipped with a digital camera (Olympus BX51M). The morphology and the crystal structure of the samples were characterized by field emission SEM (Zeiss Sigma) and XRD (Bruker D8 Advance, Cu Kα radiation). Electronic and optoelectronic properties of the devices were observed using a semiconductor parameter analyzer (Keithley 4200-SCS). A 75 W xenon arc lamp equipped with a grating monochromator (OBB PowerArc) was used as the light source. Transmittance of devices in the visible light region was obtained using a UV-vis spectrophotometer (Hitachi U-3900H).

Results and discussion

ZnO and NiO nanofibers can be synthesized using a general electrospinning method according to the literature.[25] Details are presented in the Experimental section. When using a bare glass slide as the substrate as shown in Fig. 1a, randomly arranged nanofibers were fabricated, and a majority of the nanofibers had a spring-like morphology. Optical images of the as-prepared ZnO and NiO nanofibers are displayed in Fig. 1e. To achieve uniformly aligned nanofibers, one of the most commonly used strategies is to use two parallel electrodes aside the substrate to restrict the orientation of the nanofibers.[26–28] The electric fields induced by the two assisted electrodes had opposite directions in the vicinity of the electrode edges, and could stretch the highly charged nanofibers to align perpendicular to the electrodes. However, the effects varied when this method was applied to different materials.[29,30] In our experiments, aluminum foils both connected to a negative voltage of -2 kV were employed and the glass slide was placed between them as shown in Fig. 1b. Optical images displayed in Fig. 1f indicate that the nanofibers were roughly perpendicular to the electrodes. Although most spring-like nanofibers were avoided and the nanofibers had a preferred orientation, it was obvious that the orientation distribution of the nanofibers was still rather wide.

Considering the pivotal role of the electric field induced by the two assisted electrodes, it was natural to speculate that a stronger electric field would lead to a better nanofiber alignment.[10] By simply increasing the negative high voltage, the assisted-electrode-induced electric field could be enhanced. However, the negative high voltage had a limitation in value, and higher voltage also meant more energy consumption. To avoid these disadvantages, we added the third assistant electrode between the former two electrodes as displayed in Fig. 1c. The two outside electrodes were still connected to a voltage of -2 kV while the middle one was grounded. Fig. 1g clearly shows that the alignment significantly improved for both ZnO and NiO nanofibers. The misalignment angle, as shown in Fig. 1i, was defined as the angle between a nanofiber and the normal of the assistant electrodes in our experiments. Misalignment angles of a group of nanofibers could describe overall alignment of these nanofibers quantitatively. Thus, $\sim$250 nanofibers were measured for electrospinning using two assisted electrodes and using three assisted electrodes, and the results are displayed in Fig. 1j and k. About 90% of the nanofibers distributed in $\pm 40°$
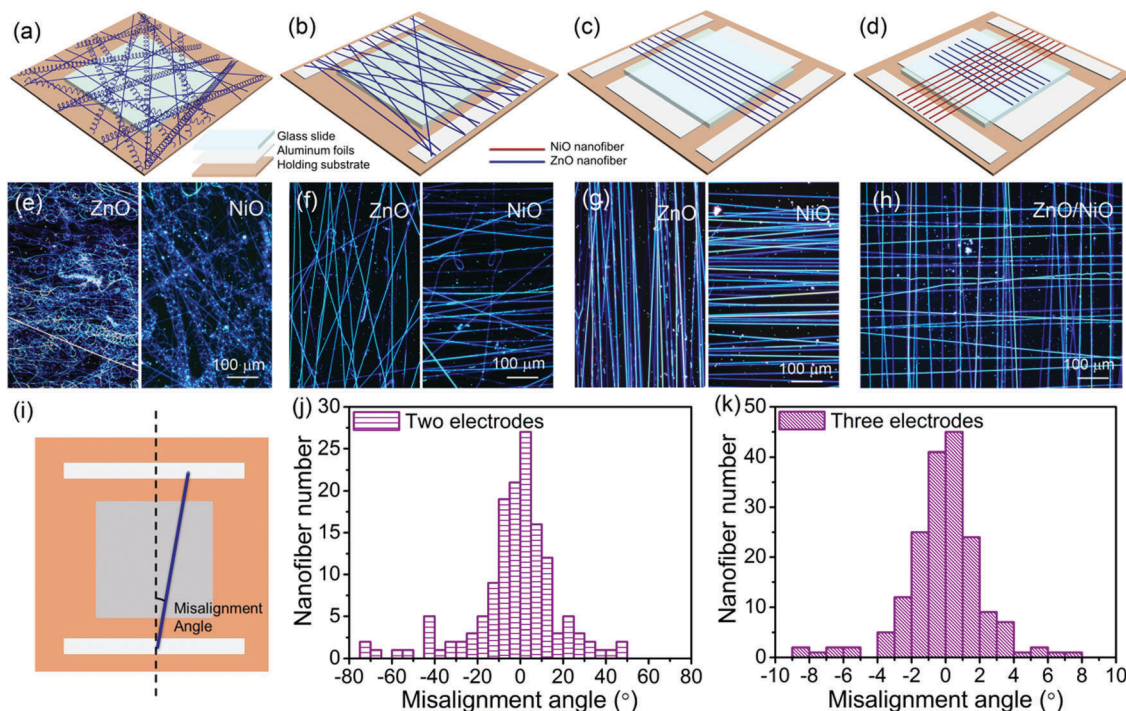
Fig. 1 Fabrication of ZnO nanofibers, NiO nanofibers and ZnO/NiO heterojunction arrays and their orientation distribution. Schematic illustration of the experimental setup for fabrication of (a) random nanofibers using no assisted electrodes, (b) roughly aligned nanofibers using two assisted electrodes, (c) uniformly aligned nanofiber arrays using three assisted electrodes and (d) ZnO/NiO heterojunction arrays. Corresponding optical images of the as-fabricated samples (e–h). (i) Definition of misalignment angles. Misalignment angles of nanofiber arrays prepared with (j) two assisted electrodes and (k) three assisted electrodes.

misalignment angles for electrospinning using two assisted electrodes. For electrospinning using three assisted electrodes, the misalignment angle range of more than 90% nanofibers dramatically decreased to $\pm 4^\circ$; meanwhile, no nanofiber was found to have a misalignment angle larger than $\pm 10^\circ$. These statistics effectively proved the improvement achieved by adding the middle electrode.

The simulative electric field distribution when using two assisted electrodes and three assisted electrodes in electrospinning is shown in Fig. S1 (ESI†). The horizontal components of the electric field at the edge of three assisted electrodes were more than one order of magnitude stronger than that of two assisted electrodes. On the other hand, the middle electrode generated an upward electrostatic force on the nanofibers which slowed the deposition of nanofibers, leading to a longer active time of the horizontal electric field on the nanofibers. The combined effects of much stronger horizontal components and additional vertical components of the electric field led to significantly improved alignment of the nanofibers. By extending the deposition time, much denser nanofiber arrays could be prepared as shown in Fig. S2 (ESI†). Also, the length of the nanofiber arrays could easily reach several millimeters with assisted electrodes of corresponding sizes, making it possible to construct large-area devices using this time-saving and low-cost method. Using this three-assisted-electrode electrospinning method, uniformly aligned ZnO nanofiber arrays were prepared followed by NiO nanofiber arrays perpendicular to them. The cross points of the ZnO and NiO

nanofibers formed ZnO/NiO heterojunction arrays as displayed in Fig. 1d and h. Details are presented in the Experimental section.

To further confirm the morphology of the prepared ZnO and NiO nanofibers, a scanning electron microscope (SEM) was used and the results are shown in Fig. 2. In agreement with the optical images shown in Fig. 1, the as-prepared ZnO and NiO nanofibers were parallel fiber arrays with an average distance between neighboring fibers of ~ 10 µm. Thus the density of ZnO/NiO heterojunction arrays was calculated to be about 10^6 cm^{-2}. Also, the heterojunction arrays had roughly even distribution on the substrate. Nanofibers and heterojunction arrays of such high density were ideal candidates to construct large area electronic devices with stable performance since a partial loss of components would have resulted in a relatively low negative effect on overall device performance. The ZnO and NiO nanofibers maintained a uniform diameter along their longitudinal direction as indicated in Fig. 2b and d, and the average diameter of the ZnO and NiO nanofibers was 182 nm and 84 nm, respectively. Both ZnO and NiO were nonporous nanofibers with a rather smooth surface. This guaranteed good adhesion of the as-prepared nanofibers to the substrate, and it also facilitated good contact between ZnO and NiO nanofibers to form reliable heterojunctions. As can be seen in Fig. 2f, NiO nanofibers on ZnO nanofibers retained the same morphology as other parts deposited directly on the substrate. Almost no breakpoints were observed for NiO nanofibers deposited on ZnO nanofibers.
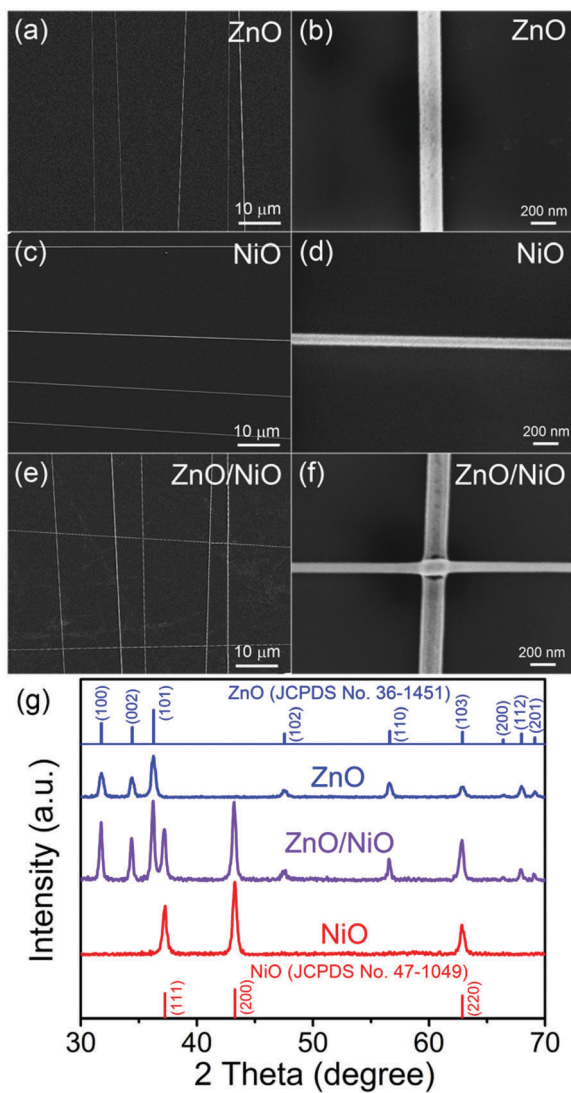
Fig. 2 Morphology and microstructure studies of the as-prepared samples. SEM images of (a and b) ZnO nanofiber arrays, (c and d) NiO nanofiber arrays and (e and f) ZnO/NiO heterojunction arrays. (g) XRD characterization of pure ZnO, pure NiO and ZnO/NiO hybrids.

To get a more clear vision of the microstructure of the as-prepared samples especially for the heterojunction arrays, X-ray diffraction (XRD) was conducted (Fig. 2g). For pure ZnO nanofibers and NiO nanofibers, only the wurtzite structure corresponding to JCPDS no. 36-1451 and the cubic structure corresponding to JCPDS no. 47-1049 were found, respectively. Note that for both ZnO and NiO nanofibers, the peaks of different lattice planes had similar intensity distributions with their standard JCPDS cards. This illustrated that the nanofibers had polycrystalline microstructures and were composed of compact crystalline grains with different orientations. For ZnO/NiO heterojunction arrays, same peaks of wurtzite ZnO and cubic NiO were identified without any unrecognized ones, which confirmed that no new structure of other crystal phases was formed at the interface of the ZnO and NiO nanofibers.

To fabricate ZnO and NiO nanofiber arrays and ZnO/NiO heterojunction arrays into devices, Cr/Au electrodes with a designed architecture were deposited using electron beam evaporation (see details in the Experimental section). For ZnO/NiO heterojunction arrays, one electrode was deposited on ZnO and the other one on NiO while keeping the two electrodes with no direct contact, as shown in the inset of Fig. 3a. The inset of Fig. 3b displays the configuration of the Cr/Au electrodes for both the ZnO nanofibers and NiO nanofibers.

A distinct rectification effect in the current–voltage (I–V) curves of the ZnO/NiO heterojunction array device could be observed in Fig. 3a. But the pure ZnO and NiO nanofiber array device had nearly linear and symmetrical I–V curves as displayed in Fig. 3b, which confirmed an approximately ohmic contact between the Cr/Au electrodes and nanofibers. Thus, the rectification effect observed in the ZnO/NiO heterojunction array device was ascribed to the built-in electric field formed at the interface between the n-type ZnO and p-type NiO nanofibers.[31,32] Under external bias, carriers traversing the device from one electrode to the other needed to go through the interface of one ZnO/NiO heterojunction. The built-in electric field also resulted in a photovoltaic effect in the device, which meant that the device had potential to work in self-powered mode without an external bias. Under illumination of 350 nm 0.753 mW cm^{-2} UV light, the ZnO/NiO heterojunction array device generated a self-powered photocurrent of 50 pA at 0 V bias. According to the band diagram shown in Fig. 3c, photo-generated electron–hole pairs in the depletion region of the ZnO/NiO heterojunction were separated and driven to opposite directions by the built-in electric field. Accumulated electrons in ZnO nanofibers and holes in NiO nanofibers would recombine in an external circuit and thus generated the self-powered photocurrent. It should be noted that the dark current at 0 V bias was 0 in theory (the measured value was at the 10^{-15} A level, reaching the measurement limit of our instrument), so the ZnO/NiO heterojunction array device could reach the best on–off ratio without an external bias on it. Our subsequent research also focused on its performance in self-powered mode.

Different from ZnO nanofiber arrays of which the on–off ratio was ∼20 under 350 nm 0.753 mW cm^{-2} UV light at 0.5 V, NiO nanofiber arrays generated no photocurrent in the measurement although they had a matched band gap[33,34] with incident light (Fig. 3b). On one hand, a large amount of grain boundaries and surface defects served as recombination centers in NiO nanofibers. Some of the photo-generated carriers would soon recombine during their transport, resulting in rather short average excess carrier lifetime. On the other hand, NiO nanofibers in the device had a length of several millimeters, and photo-generated carriers could not transport such a long distance to reach the electrodes. Thus, no difference between dark current and light current could be measured.

Due to the low speed of oxygen adsorption and desorption on the surface, ZnO nanomaterial based PDs normally have a long response time such as tens of seconds.[35–37] The as-prepared ZnO nanofiber array device also had a response time of 19.5 s for the current rise and 45.2 s for the current decay at 5 V bias, as shown in Fig. 3e. For the ZnO/NiO heterojunction array PD, the rise time and the decay time observably decreased to 7.5 s and 4.8 s respectively at 0 V bias (Fig. 3d). In particular, the decay time
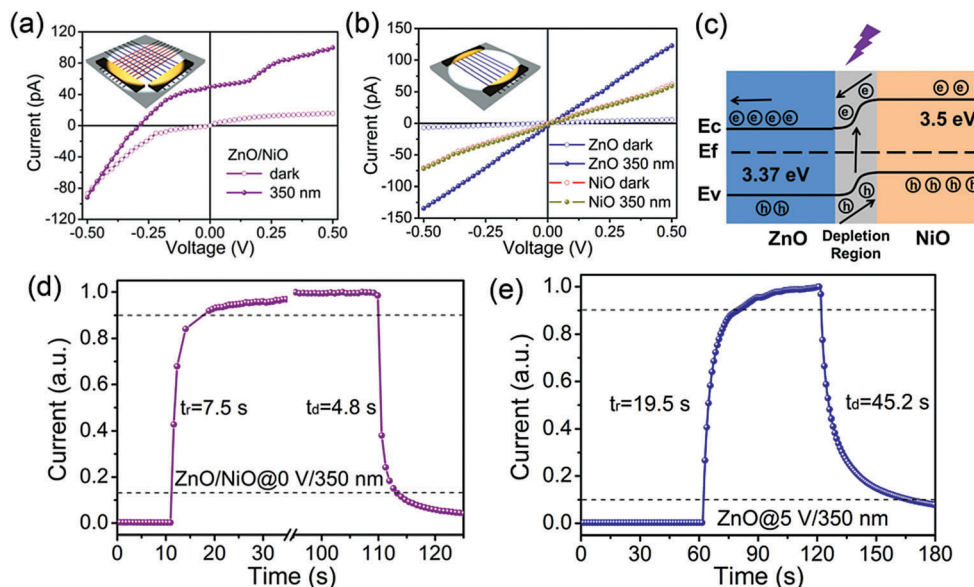
Fig. 3 Optoelectronic performance of the as-fabricated devices. $I-V$ curves of the (a) ZnO/NiO heterojunction array PD and the (b) ZnO and NiO nanofiber array device in the dark and under 350 nm UV light. The inset displayed the device configuration of the ZnO/NiO heterojunction arrays and both ZnO and NiO nanofiber arrays. (c) Band diagram of ZnO/NiO heterojunctions showing the generation and transfer processes of electron−hole pairs in depletion regions and ZnO nanofibers under UV illumination at 0 V bias. The response speed of the (d) ZnO/NiO heterojunction array PD at 0 V bias and the (e) ZnO nanofiber array device at 5 V bias.

decreased to almost one tenth that of the ZnO nanofiber array device. As explained before, the depletion region of the ZnO/NiO heterojunction played a key role in self-powered mode. Upon illumination, photo-generated electron–hole pairs in the depletion region were separated and swept into the external circuit quickly by the built-in electric field, resulting in fast-increasing light current. Once the incident light was turned off, the power supply for electron transition stopped and the carrier density in the depletion region decreased rapidly so that the device current dropped to a dark level in a short time.

For a UV PD, spectrum selectivity is one of the most important characteristics. To evaluate the performance of our ZnO/NiO heterojunction array PD, responsivity at 0 V bias was calculated from the following equation:[38] $R_\lambda = (I_{light} - I_{dark})/PS$, where λ, I_{light}, I_{dark}, P, and S were the wavelength of incident light, the light current, the dark current, the power density of incident light, and the effective area of the device under illumination. A cutoff edge at 370 nm could be identified in Fig. 4a, and the UV-visible rejection ratio[39] (R_{300nm}/R_{400nm}) of this device was about 44. The high rejection ratio and the sharp cutoff edge of this device confirmed its perfect UV spectrum selectivity, indicating it to be an ideal candidate for UV photodetection.

Responsivity of a UV PD also implies its ability to generate electric signals under certain illumination and bias conditions, especially for PDs working in self-powered mode. The ZnO/NiO heterojunction array PD reached a maximum R_λ of 0.415 mA W^{-1} at 0 V bias under the illumination of 300 nm 0.406 mW cm^{-2} UV light in the 300–600 nm incident light wavelength region. This was much higher compared with recently reported PDs based on TiO$_2$/NiO or MgZnO/polyaniline film heterojunctions.[40,41] The high responsivity was mainly ascribed to the discrete configuration of ZnO/NiO

heterojunction arrays which allowed more UV light to reach the depletion region directly; while for heterojunctions of stacked films, UV light needed to pass through the upper layer film before reaching the heterojunction interface. Note that all nanofibers were calculated in effective area of our device under illumination while ZnO/NiO heterojunctions played a major role in photocurrent generation at 0 V bias. If the effective area was calculated as the area of ZnO/NiO heterojunctions only, the responsivity of this ZnO/NiO PD would be much higher than that shown above.

Fig. 4b shows the response of different devices to periodically on–off UV illumination. The ZnO/NiO heterojunction array device exhibited a good stability as its light current remained stable and unchanged in all five cycles. And this was mainly guaranteed by the following two reasons: (1) compact grains with no holes in the nanofibers guaranteed reliable contact between ZnO and NiO nanofibers as well as between nanofibers and the substrate; (2) devices based on ZnO/NiO heterojunction arrays with a density of ∼10^6 cm^{-2} had high tolerance to partial failure. A much lower response current to UV light was also observed for the ZnO nanofiber array PD at 0 V bias. As mentioned before, the weak photovoltaic effect arose from the imperfect ohmic contact between the ZnO nanofibers and Cr/Au electrodes should be the main reason.[42–44] We also studied the current response of the ZnO/NiO PD to UV light of different power densities, as shown in Fig. 4c. It was concluded that the device had a stable response with the same speed to light of different power densities. The inset of Fig. 4c displays a nonlinear relationship between photocurrent and power density, which suggested a complex process of electron–hole generation, recombination, and trapping within the device.[45,46]

With the average diameters of ZnO and NiO nanofibers being 182 nm and 84 nm respectively and the average distance

This journal is © The Royal Society of Chemistry 2019

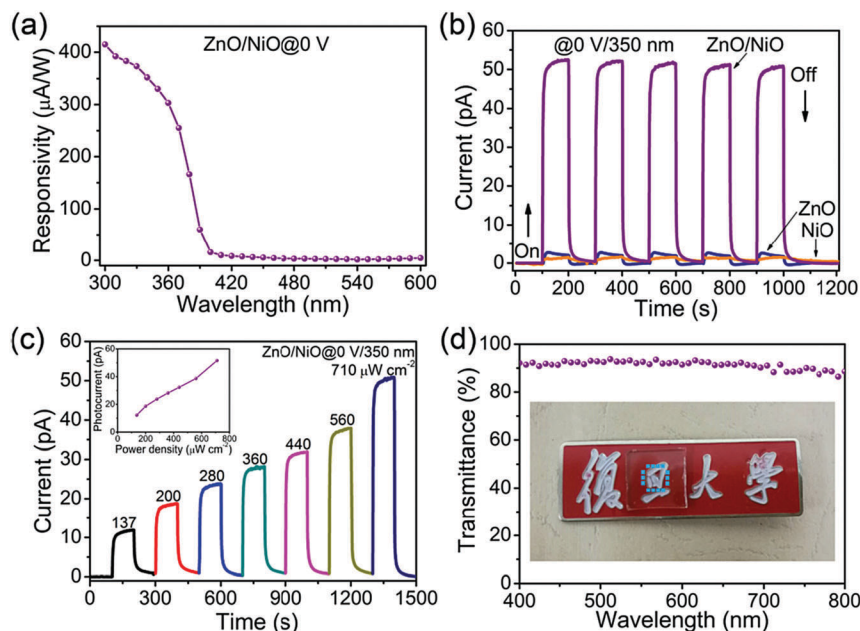*J. Mater. Chem. C*, 2019, **7**, 223–229 | **227**

Fig. 4   Optoelectronic performance of the self-powered ZnO/NiO heterojunction array PD. (a) Responsivity of the ZnO/NiO heterojunction array UV PD as a function of incident light wavelength. (b) On−off switching tests of the as-fabricated devices at 0 V under 350 nm light. (c) On−off test of the ZnO/NiO heterojunction array PD to 350 nm light with different power densities. The inset displayed a nonlinear relationship between photocurrent and power density. (d) Transmittance of the ZnO/NiO heterojunction array PD (including the glass slide substrate) in the visible light region. The inset shows a photo of the device with the second Chinese character of Fudan University under it.

between neighboring fibers being ∼10 μm, only less than 3% of the substrate was covered by ZnO/NiO heterojunction arrays. Now that the glass slide was transparent in the visible light region (Fig. S3, ESI†), the ZnO/NiO PD possessed great potential in being a transparent electronic device. Fig. 4d displays the transmittance of the ZnO/NiO PD (including the glass slide substrate) in the 400–800 nm wavelength range. The device had an average transmittance of 90% in characterization, which only decreased slightly compared with a bare glass slide. An intuitive photo is shown in the inset of Fig. 4d, and the second Chinese character of Fudan University could be identified clearly beneath the device. These results effectively proved our ZnO/NiO device to be a high-performance transparent UV PD.

Conclusions

In summary, a modified electrospinning method was proposed and applied for the fabrication of high-performance self-powered UV PDs based on highly ordered ZnO/NiO heterojunction arrays with a density of 10^6 cm^{-2}. The as-prepared ZnO and NiO nanofiber arrays of several millimeters long had more than 90% of the nanofibers aligned to within ±4° of the desired direction, which was mainly attributed to the strong and properly distributed electric field induced by the three assisted electrodes. The ZnO/NiO heterojunction array UV PD had a maximum responsivity of 0.415 mA W^{-1} and a short rise/decay time of 7.5 s/4.8 s at 0 V bias, which was greatly improved compared with the reference ZnO nanofiber array device. The built-in electric field of the ZnO/NiO heterojunction arrays, which introduced a photovoltaic effect and

enhanced the charge separation efficiency of photo-generated carriers, was considered as the main reason for the improvement. Also, the ZnO/NiO PD was fully transparent in the visible light region with an average transmittance of 90%. This modified electrospinning method using three assisted electrodes had potential in fabricating uniformly aligned nanofiber arrays of different materials, which could be further used as building blocks for novel nanostructures and high-performance functional devices.

Conflicts of interest

There are no conflicts to declare.

Acknowledgements

Notes and references

1 W. Lu and C. M. Lieber, *Nat. Mater.*, 2007, **6**, 841–850.
2 M. C. P. Wang and B. D. Gates, *Mater. Today*, 2010, **12**, 34–43.

3 X. S. Fang, Y. Bando, M. Liao, T. Zhai, U. K. Gautam, L. Li, Y. Koide and D. Golberg, *Adv. Funct. Mater.*, 2010, **20**, 500–508.

4 W. X. Ouyang, F. Teng and X. S. Fang, *Adv. Funct. Mater.*, 2018, **28**, 1707178.

5 W. Yang, K. Hu, F. Teng, J. H. Weng, Y. Zhang and X. S. Fang, *Nano Lett.*, 2018, **18**, 4697–4703.

6 Y. Liu, X. Zhang, Y. Xia and H. Yang, *Adv. Mater.*, 2010, **22**, 2454–2457.

7 M. Li, Y.-Z. Long, D. Yang, J. Sun, H. Yin, Z. Zhao, W. Kong, X. Jiang and Z. Fan, *J. Mater. Chem.*, 2011, **21**, 13159–13162.

8 Y. Wu, L. A. Carnell and R. L. Clark, *Polymer*, 2007, **48**, 5653–5661.

9 G. Cadafalch Gazquez, S. Lei, A. George, H. Gullapalli, B. A. Boukamp, P. M. Ajayan and J. E. Ten Elshof, *ACS Appl. Mater. Interfaces*, 2016, **8**, 13466–13471.

10 Y. Ning, Z. Zhang, F. Teng and X. S. Fang, *Small*, 2018, **14**, 1703754.

11 X. Ma, M. Xue, F. Li, J. Chen, D. Chen, X. Wang, F. Pan and G. F. Chen, *Nanoscale*, 2015, **7**, 8715–8719.

12 M. Xue, Z. Xie, L. Zhang, X. Ma, X. Wu, Y. Guo, W. Song, Z. Li and T. Cao, *Nanoscale*, 2011, **3**, 2703–2708.

13 B. Sun, Y.-Z. Long, S.-L. Liu, Y.-Y. Huang, J. Ma, H.-D. Zhang, G. Shen and S. Xu, *Nanoscale*, 2013, **5**, 7041–7045.

14 F. Teng, K. Hu, W. X. Ouyang and X. S. Fang, *Adv. Mater.*, 2018, **30**, 1706262.

15 J. Yao, H. Yan and C. M. Lieber, *Nat. Nanotechnol.*, 2013, **8**, 329–335.

16 N. Nasiri, R. Bo, F. Wang, L. Fu and A. Tricoli, *Adv. Mater.*, 2015, **27**, 4336–4343.

17 H. Kind, H. Yan, B. Messer, M. Law and P. Yang, *Adv. Mater.*, 2002, **14**, 158–160.

18 W. Ouyang, F. Teng, M. Jiang and X. S. Fang, *Small*, 2017, **13**, 1702177.

19 F. Teng, W. Ouyang, Y. Li, L. Zheng and X. S. Fang, *Small*, 2017, **13**, 1700156.

20 B. Nie, J. Hu, L. Luo, C. Xie, L. Zeng, P. Lv, F. Li, J. Jie, M. Feng and C. Wu, *Small*, 2013, **9**, 2872–2879.

21 S. M. Hatch, J. Briscoe and S. Dunn, *Adv. Mater.*, 2013, **25**, 867–871.

22 W. Tian, T. Zhai, C. Zhang, S. L. Li, X. Wang, F. Liu, D. Liu, X. Cai, K. Tsukagoshi and D. Golberg, *Adv. Mater.*, 2013, **25**, 4625–4630.

23 P. Ni, C. Shan, S. Wang, X. Liu and D. Shen, *J. Mater. Chem. C*, 2013, **1**, 4445–4449.

24 Y. Chen, Y. Lu, C. Lin, Y. Tian, C. Gao, L. Dong and C. Shan, *J. Mater. Chem. C*, 2018, **6**, 5727–5732.

25 D. Lin, H. Wu, R. Zhang and W. Pan, *Chem. Mater.*, 2009, **21**, 3479–3484.

26 D. Li and Y. Xia, *Adv. Mater.*, 2004, **16**, 1151–1170.

27 D. Li, Y. Wang and Y. Xia, *Nano Lett.*, 2003, **3**, 1167–1171.

28 D. Li, G. Ouyang, J. T. McCann and Y. Xia, *Nano Lett.*, 2005, **5**, 913–916.

29 D. Lin, H. Wu and W. Pan, *Adv. Mater.*, 2007, **19**, 3968–3972.

30 S. H. Choi, G. Ankonina, D. Y. Youn, S. G. Oh, J. M. Hong, A. Rothschild and I. D. Kim, *ACS Nano*, 2009, **3**, 2623–2631.

31 B. Sasi, K. G. Gopchandran, P. K. Manoj, P. Koshy, P. P. Rao and V. K. Vaidyan, *Vacuum*, 2002, **68**, 149–154.

32 Z. Zhang, C. Shao, X. Li, C. Wang, M. Zhang and Y. Liu, *ACS Appl. Mater. Interfaces*, 2010, **2**, 2915–2923.

33 N. P. Klochko, V. R. Kopach, I. I. Tyukhov, D. O. Zhadan, K. S. Klepikova, G. S. Khrypunov, S. I. Petrushenko, V. M. Lyubov, M. V. Kirichenko, S. V. Dukarov and A. L. Khrypunova, *Sol. Energy*, 2018, **164**, 149–159.

34 N. Nasiri, R. Bo, L. Fu and A. Tricoli, *Nanoscale*, 2017, **9**, 2059–2067.

35 C. Soci, A. Zhang, B. Xiang, S. A. Dayeh, D. P. R. Aplin, J. Park, X. Y. Bao, Y. H. Lo and D. Wang, *Nano Lett.*, 2007, **7**, 1003–1009.

36 Y. Jin, J. Wang, B. Sun, J. C. Blakesley and N. C. Greenham, *Nano Lett.*, 2008, **8**, 1649–1653.

37 K. Liu, M. Sakurai, M. Liao and M. Aono, *J. Phys. Chem. C*, 2010, **114**, 19835–19839.

38 X. Xu, J. Chen, S. Cai, Z. Long, Y. Zhang, L. Su, S. He, C. Tang, P. Liu, H. Peng and X. S. Fang, *Adv. Mater.*, 2018, **30**, 1803165.

39 B. Zhao, F. Wang, H. Chen, L. Zheng, L. Su, D. Zhao and X. S. Fang, *Adv. Funct. Mater.*, 2017, **27**, 1700264.

40 L. Zheng, F. Teng, Z. Zhang, B. Zhao and X. S. Fang, *J. Mater. Chem. C*, 2016, **4**, 10032–10039.

41 H. Chen, P. Yu, Z. Zhang, F. Teng, L. Zheng, K. Hu and X. S. Fang, *Small*, 2016, **12**, 5809–5816.

42 H. Chen, K. Liu, X. Chen, Z. Zhang, M. Fan, M. Jiang, X. Xie, H. Zhao and D. Shen, *J. Mater. Chem. C*, 2014, **2**, 9689–9694.

43 Z. Bai, X. Chen, X. Yan, X. Zheng, Z. Kang and Y. Zhang, *Phys. Chem. Chem. Phys.*, 2014, **16**, 9525–9529.

44 R. Chen, C. Chen, H. Tsai, W. Wang and Y. Huang, *Appl. Phys. Lett.*, 2012, **100**, 123108.

45 H. Liu, Z. Zhang, L. Hu, N. Gao, L. Sang, M. Liao, R. Ma, F. Xu and X. S. Fang, *Adv. Opt. Mater.*, 2014, **2**, 771–778.

46 G. Liu, N. Hoivik, X. Wang, S. Lu, K. Wang and H. Jakobsen, *Electrochim. Acta*, 2013, **93**, 80–86.

This journal is © The Royal Society of Chemistry 2019

J. Mater. Chem. C, 2019, **7**, 223–229 | **229**